



HAL
open science

Detection, quantification, and characterization by whole-slide image analysis of bacterial infection by *Vibrio aestuarianus*, stained by immunohistochemistry, in the pacific oyster *Magallana gigas*

Valentin Geslin, Luca Tomasetti, Thor Ole Gulsrud, Leila Parizadeh,
Marie-Agnes Travers

► **To cite this version:**

Valentin Geslin, Luca Tomasetti, Thor Ole Gulsrud, Leila Parizadeh, Marie-Agnes Travers. Detection, quantification, and characterization by whole-slide image analysis of bacterial infection by *Vibrio aestuarianus*, stained by immunohistochemistry, in the pacific oyster *Magallana gigas*. *Aquaculture*, 2025, 598, pp.741983. 10.1016/j.aquaculture.2024.741983 . hal-04829499

HAL Id: hal-04829499

<https://hal.science/hal-04829499v1>

Submitted on 10 Dec 2024

HAL is a multi-disciplinary open access archive for the deposit and dissemination of scientific research documents, whether they are published or not. The documents may come from teaching and research institutions in France or abroad, or from public or private research centers.

L'archive ouverte pluridisciplinaire **HAL**, est destinée au dépôt et à la diffusion de documents scientifiques de niveau recherche, publiés ou non, émanant des établissements d'enseignement et de recherche français ou étrangers, des laboratoires publics ou privés.

Detection, quantification, and characterization by whole-slide image analysis of bacterial infection by *Vibrio aestuarianus*, stained by immunohistochemistry, in the pacific oyster *Magallana gigas*

Valentin Geslin ^{a,*}, Leila Parizadeh ^b, Marie-Agnès Travers ^c, Luca Tomasetti ^d, Thor Ole Gulsrud ^e

^a *University of Stavanger, Faculty of Science and Technology, Department of Chemistry, Bioscience and Environmental Engineering, Norway*

^b *Littoral Environnement et Sociétés (LIENSs), UMRi, 7266, CNRS, La Rochelle Université, 2 rue Olympe de Gouges, 17000 La Rochelle, France*

^c *IHPE, Univ Montpellier, CNRS, IFREMER, Univ Perpignan Via Domitia, Montpellier, France*

^d *University of Stavanger, Faculty of Science and Technology, Department of Electrical Engineering and Computer Science, Norway*

^e *University of Stavanger, Faculty of Health Sciences, Department of Quality and Health Technology, Norway*

KEYWORDS

Digital histopathology - Immunohistochemistry - *Magallana gigas* - *Vibrio aestuarianus* - Whole slide image

ABSTRACT

The growth of marine bivalve aquaculture is presented as a potential measure to effectively provide seafood for human consumption while preserving wild populations. It can be an economic driver in coastal areas while also providing important ecosystem services such as filtration of phytoplankton and carbonate buffering. However, as with other farming practices, increased densities of individuals in a confined space often results in disease outbreaks. Pathogens developing under these conditions can easily spread among farmed stocks, affecting some or possibly most or all production lines, potentially causing adverse economic consequences on the local aquaculture sector, spreading over large areas and eventually affecting wild populations as well. Development and implementation of early detection methods for pathogen infection are imperative to maintain and expand aquaculture activities. In this context, a new method to quantify and characterize infection by *Vibrio aestuarianus* in the Pacific oyster, *Magallana gigas*, based on whole-slide image analysis of histological slides stained by immunohistochemistry is presented. The method is used to automatically measure the proportion of tissue infected by IHC-stained bacteria from each image and to characterize bacteria spread in the tissue. The proportion of tissue infected by IHC-stained bacteria and spatial dispersion indexes, used to characterize 2D bacterial dispersion, were generally associated with the quantity of bacteria previously measured by quantitative polymerase chain reaction (qPCR). These results suggest a pattern of infection where *V. aestuarianus* tends to be more clustered and less randomly spread in the organism with increased infection. Advantages, limitations, and potential ways to improve the method are discussed.

1. Introduction

Emerging pathogens represent one of the most significant threats to the growth and sustainability of aquaculture industries worldwide (Lupo et al., 2016) and the outbreak of aquatic animal diseases related to intensive production practices is of major concern for the industry, as well as for other members of local communities depending on aquaculture economy, and other resources from the ecosystem (Boyd and Clay, 1998; Griffiths et al., 2018; Landos et al., 2021). Past severe disease outbreaks have led to significant economic destruction and negative social consequences (Carnegie et al., 2016). Disease outbreaks often occur from a combination of different factors such as climate change (Barange et al., 2018; Garrabou et al., 2022; Li et al., 2023; Wright et al., 2023), environmental pollution (Kalkan and Altug, 2020; Kathijotes et al., 2015; Landos et al., 2021), habitat alteration (Barange et al., 2018), geographic expansion of disease (Barange et al., 2018; Carnegie et al., 2016), and invasive species (Green et al., 2016; Wright et al., 2023; Yang et al., 2021). Aquaculture practices, which confine animals at high density in specific areas, and often involve manipulation and transfer of farmed animals from one location to another, are another source of stress that can result in conditions conducive to the outbreak and propagation of infectious agents (Ben-Horin et al., 2018; Carnegie et al., 2016; Palacios et al., 2010). All these factors can directly impact the prevalence and severity of disease outbreaks in both farmed and wild aquatic populations (Landos et al., 2021). With the growth of the world population, bivalve molluscan farmers are a key sector due to the importance of these protein-rich animals for human consumption. In this context, aquaculture can play a strategic role in terms of safe food production, and sustainable economic and social development (Noger- Huet et al., 2022; Petrosillo et al., 2023). The development of new methods for disease detection in marine shellfish is essential to detect diseases as early as possible and apply contingency measures to contain their spread to other aquaculture facilities (Carnegie et al., 2016).

The Pacific oyster *Magallana gigas*, indigenous to Northeast Asia, is the most cultivated species in the world (Chaney and Gracey, 2011), including France, where the yearly production in 2022 was estimated at 85,000 tons (FAO, 2022). Since the early 1990s, Pacific oysters have been affected by disease-induced mass mortality events in many parts of the world (Arzul et al., 2017; Burge et al., 2017; Castinel et al., 2015; Berg et al., 2015; McCombie and Samain, 2007). These disease outbreaks, either due to the presence of the virus OsHV-1 or the bacteria *Vibrio aestuarianus*, have had major impacts on oyster production in France and also in other parts of Europe (Berg et al., 2015). Alarmingly, the prevalence of these outbreaks in European oyster populations appears to have increased in recent decades (Ax'én et al., 2019). Consequences of infection by *V. aestuarianus* on *M. gigas* range from non-lethal to lethal effects, leading to behavioral change (Elston, 1993), pathological reaction (Garnier et al., 2007), and ultimately to death (Parizadeh et al., 2018a). Oysters are frequently moved between spat collection sites and oyster farming sites within the same country, but also between different countries (Arzul et al., 2022). Therefore, the lack of effective transport control and early disease detection methods can contribute to the widespread transmission of pathogenic agents (Carnegie et al., 2016; Fuhrmann et al., 2019). In this context, the development of new methods allowing early detection and accurate diagnosis of infectious diseases is one of the major goals of the aquaculture sector. The main detection methods currently used to assess *V. aestuarianus* infection in *M. gigas* are histopathological diagnosis together with strain identification by polymerase chain reaction (PCR) and qPCR assays to quantify infection level (Ax'én et al., 2019). Nevertheless, due to the short incubation time of the pathogenic agent and the increase in its prevalence, it remains difficult to detect early signs of large-scale episodes of infection by conventional surveillance methods (Parizadeh et al., 2018a; Paul-Pont et al., 2013; Whittington et al., 2019).

Whole slide image (WSI) analysis is rapidly evolving and increasingly used in histopathology as it enables high throughput analysis of a large number of samples, offering the potential for increased diagnostic precision, improved reproducibility, and potentially reduced workload for histopathologists (Zarella et al., 2019). Production of WSI involves the scanning of a microscope slide to create a single high-resolution digital file. WSI are pyramidal images of histological slides containing complex data. They have a higher resolution compared to raster graphic files allowing the detection of cellular or even sub-cellular structures (Bolte and Cordelieres, 2006; Pantanowitz et al., 2011). Whole slide imaging represents a paradigm shift in histopathology with potential impacts on workflows,

reproducibility, dissemination, and intra and inter-institutional collaboration (Bolte and Cordelières, 2006). Although the benefits of WSI analysis are numerous, implementing such methods on routine procedures remains slow because it requires some adaptation and the complexity of the data is still an obstacle to its widespread adoption (Aeffner et al., 2019).

In this article, a method to detect, quantify, and characterize *V. aestuarianus* infection of *M. gigas* from WSI stained by immunohistochemistry (IHC) is proposed. *M. gigas* were experimentally infected with *V. aestuarianus* to control and create different degrees of infection (Parizadeh et al., 2018a). The method is based on the computerized detection in WSI of *V. aestuarianus* stained by IHC. The proportion of tissue infected by IHC-stained bacteria is measured and spatial dispersion of the bacteria in the image is characterized. Bacterial quantities assessed with this method are generally consistent with results obtained by qPCR and the method brings new details on bacterial proliferation through host tissues.

2. Materials & methods

WSI and qPCR results originated from Parizadeh et al., 2018b. WSIs were produced to assess histopathological damage in *M. gigas* infected under experimental conditions by *V. aestuarianus* against the degree of bacterial infection assessed by quantitative qPCR and IHC with the use of a polyclonal antibody (Parizadeh et al., 2018a). To briefly summarise the protocol from Parizadeh et al., 2018a, adult *M. gigas* were exposed for 24 h to either contaminated seawater containing bacteria (5×10^8 bacterial cells L^{-1}), or UV-treated seawater as a control. After this initial exposure, infected and controlled oysters were transferred to new tanks containing UV-treated seawater and sampled on days 1 and 4 post-exposure to assess bacterial infection. Animals were dissected in a clean environment with alcohol-rinsed instruments. Histopathological lesions and the presence of IHC-stained *V. aestuarianus* in different tissues were assessed visually on histological slides stained with hematoxylin-eosin (H&E) and on slides stained by IHC with a bacteria-specific polyclonal antibody. DNA quantification by qPCR was performed on 230 different tissue samples (gills, digestive gland, mantle, abductor muscle, labial palp) from 43 specimens. Total DNA was extracted using the QiaAmp® kit (Qiagen) according to the manufacturer's instructions. The quality and quantity of genomic DNA were determined by measuring the optical density at 260 and 280 nm using the NanoDrop (Thermo). The DNA concentration was subsequently adjusted to 5 ng/ μ l. Quantification of *V. aestuarianus* DNA levels was carried out using dnaJ qPCR (Saulnier et al., 2009) on the MX3000 and MX3005 thermocycler (Agilent) using Brilliant III Ultrafast kit for Taqman technology (Stratagene). Each reaction was performed in duplicate in a volume of 20 μ l containing 200 nM of each primer (dnaJ F: GTATGAAATTTTAACTGACCCACAA, dnaJ R: CAATTTCTTTGCAACAACCAC), 200 nM of an oligonucleotide probe (dnaJ probe TGGTAGCGCAGACTTCGGCGAC) and 5 μ l of DNA using the following protocol: initial denaturation for 3 min at 95 °C followed by 40 cycles of amplification (10 s at 95 °C and 20 s at 60 °C).

The qPCR results were treated individually by tissue and the overall mean was calculated for every specimen. Logarithm-transformed values were used for qPCR values. Only specimens with both WSI and qPCR data were integrated into the current analysis ($n = 38$).

Samples were classified into 3 infection groups according to the level of bacteria measured by qPCR, with the “control group” encompassing every control specimen, samples with a level of bacteria cells per animal ranging from 0 to 1.10^5 bacteria/25 ng of total DNA fall into “early infection group”, and “advanced infection group” encompass samples presenting a level of bacteria cells above 1.10^5 bacteria per 25 ng of total DNA. See Table 3 and Fig. A in 7.0 Supplementary Material.

Original WSI and qPCR data can be found here: <https://www.seanoe.org/data/00501/61299/>.

Software used for image analysis were QuPath (0.5.1), Python (3.11.5), and Fiji (2.15.0). QuPath is an open-source bioimage analysis software for digital pathology and WSI analysis (<https://qupath.github.io/>). Python is a general-purpose, object-oriented programming language, it offers a comprehensive standard library to work on different

types of objects (<https://www.python.org/>). Fiji is an image processing package distribution of ImageJ2 (<https://imagej.net/software/fiji/>).

Tissue detection was performed using a thresholding method in QuPath. Pixel dimensions were exported from QuPath for each WSI's metadata. Tiles of a specific size ($400 \mu\text{m}^2$) with a downsampling factor of 1 were generated within the area of tissue detected for each WSI and exported as raster graphics files. Tiles were converted from RGB to HSV, and a lower and upper color threshold corresponding to IHC stained color were defined. Color thresholding was performed on each tile to obtain a binary mask to select only pixels within the range defined by lower and upper values. Black pixels are the pixels falling outside the defined color range and therefore were assumed to represent tissue with no IHC-stained bacteria present, while non-black pixels are the pixels falling within the IHC color threshold range and were assumed to represent tissue infected by IHC-stained bacteria. Some tiles from different tissues and their respective masks are presented in [Table 1](#). The number of non-black pixels was exported for every masked tile. The area of tissue infected by IHC-stained bacteria was calculated by multiplying the number of non-black pixels by the pixel dimensions for all tiles and summing them for each image. Specimens from "control" were assumed not to have been infected by *V. aestuarianus*, all the traces of IHC detected in these samples were considered artifacts. Therefore IHC-stained bacteria areas were corrected by subtracting the highest area measured in the "control" group from every sample.

WSIs were exported as raster images with HistoQC ([Janowczyk et al., 2019](#)). HistoQC is an open-source tool written in Python used to identify artifact-free areas on digitized slides. These images were used to characterize IHC-stained bacteria colocalization and spatial dispersion within the whole cross-section. Particle distribution analysis statistically determines if particles in each image are likely to be randomly distributed, self-avoiding, or clustered. The "2D Particle Distribution" function from the BioVoxel plugin was used to characterize IHC stained particle spatial dispersion within the images ([Brocher, 2022](#)). It calculates the nearest neighbor distance (NND) for each particle and computes the theoretical mean NND. The measured mean NND is used as a cluster index as it represents the average minimal distance between IHC-stained bacteria and therefore if bacteria tend to form clusters or not. The standard deviation of the mean NND is informative about spatial dispersion homogeneity, or if particles tend to be clustered (lower standard deviation) or randomly dispersed (higher standard deviation). The measured mean NND was statistically compared using a *t*-test to the theoretical mean NND to determine particle distribution ([Lagache et al., 2015](#)). The general workflow of the WSI analysis method is shown in [Fig. 1](#).

Statistical analysis was performed using R (version 4.3.1). A 0.05 significance level was used for all statistical tests. Wilcoxon test is a non-parametric test used to determine if two independent groups present a significant difference in their median value. Wilcoxon test was used to determine if the median of the distribution from the proportion of tissue infected by IHC stained bacteria, mean quantity of bacteria cells, mean NND and spatial dispersion indexes were significantly different from 0. Kruskal-Wallis test followed by Dunn's test was used to compare the proportion of tissue infected by IHC-stained bacteria, mean NND, and spatial dispersion index, between infection groups. The Kruskal-Wallis test is a non-parametric test used to reveal statistically significant differences between the medians of several independent groups. Dunn's test performs pairwise comparisons between each independent group and tells which groups are significantly different. Kendall correlation test was used to assess the linear relationship between bacterial quantity and, the proportion of tissue infected by IHC-stained bacteria in each image as well as the relationship between the proportion of tissue infected by IHC-stained bacteria and with spatial dispersion index. Logarithmic regressions were used to model the relationship between the mean quantity of bacteria (\log_{10}) per sample, as a predictor variable, the proportion of tissue infected by IHC-stained bacteria, as well as the relationship between the proportion of tissue infected by IHC-stained bacteria and the dispersion index. The F-value tells whether the regression model provides a better fit to the actual data than a model with no predictor variables. All scripts used for image and data analysis are available on the following repository: <https://github.com/Valentin-Geslin/oyster>.

Colocalization is the spatial correlation between objects, it reveals whether different objects are localized within a certain area or not. It was used to assess if detected IHC-stained bacteria were localized within the tissue of interest or not. Characterization of IHC-stained bacteria colocalization within the whole tissue was performed on Fiji with the JaCoP plugin using an object-based colocalization measurement (Bolte and Cordelières, 2006). Object-based colocalization measurements refer to a colocalization method where objects of interest are first segmented from the image, then their spatial relationships are measured. This type of colocalization method was used because it is generally considered less sensitive to image noise and statistically more robust than pixel-based methods (Lagache et al., 2015). Pearson's correlation coefficient was used to express the correlation between colocalized objects representing IHC-stained bacteria with the tissue, and the linear equation describing the relationship between objects in IHC-detected images and mask tissue images was calculated by a linear regression with the slope of the regression providing the rate of association between the objects (Brocher, 2022). Pearson's coefficient provides an estimate of the goodness of this approximation with its value ranging from 1 to - 1, with 1 standing for complete positive correlation, 0 standing for no correlation, and - 1 for a negative correlation (Lagache et al., 2015). Pearson's correlation coefficient represents the degree of colocalization.

3. Results

3.1. Quantity of bacteria in whole organisms

The whole organism infection level was calculated as the mean of the individual quantities measured by qPCR in each of the tissues (gills, digestive gland, mantle, muscle, and labial palp). The 3 conditions (control, early infection and advanced infection) reflect the quantity of bacteria distribution (Fig. A - Supplementary Material) and they exhibit significant differences between them (Kruskal-Wallis test, p -value <0.05) with the "control" group presenting a median quantity of bacteria cells per animals not significantly different from 0 (Wilcoxon test, p -value >0.05) while the median quantity of bacteria cells per animals for "early infection" and "advanced infection" group were significantly higher than "control" group (Dunn's test, p -value <0.05), with a median value of 0.46 for "early infection" group and 6.93 for "advanced infection" group (Fig. 2).

3.2. Proportion of tissue infected by IHC-stained bacteria

The median value of the proportion of tissue infected by IHC-stained bacteria was significantly higher than 0 (Wilcoxon test, p -value <0.05) for the 3 categories, with the "advanced infection" group being significantly higher than the two other groups (Dunn's test, p -value <0.05). "Control" and "early infection" groups display the proportion of tissue infected by IHC-stained bacteria ranging from 0 % to 0.09 %, while the proportion of tissue infected by IHC-stained bacteria for the "advanced infection" group ranged from 1.47 % to 26.53 %, with a median value of 9.19 % (Fig. 2).

3.3. Relationship between quantity of bacteria and proportion of tissue infected by IHC stained bacteria per sample

A Spearman's rank correlation was used to test the strength and direction of the relationship between the proportion of tissue infected by IHC-stained bacteria and the mean quantity of bacteria measured by qPCR. A significant positive correlation was found between these two variables ($\tau = 0.59$, p -value <0.05). To better describe the monotonic relationship between the area of tissue infected by IHC-stained bacteria and the mean quantity of bacteria per sample the following logarithmic regression model was fitted to the data:

$$y = 3.42 + 0.59 \cdot \ln(x)$$

The overall F-value of the model was 43.91 (p -value <0.05) with an adjusted R squared of 0.53 (Fig. 3).

3.4. Spatial characterization of IHC-stained bacterial infection

3.4.1. Colocalization

The colocalization coefficient ranged from -0.006 to 0.356 with a median value of 0.007 . Individual values can be found in Table 3 in 7.0 Supplementary Material. The median of Pearson's correlation coefficient exhibits significant difference between the 3 groups (Kruskal- Wallis, p -value <0.05). The median colocalization index for the "control" and "early infection" group was not significantly different from 0 (Wilcoxon test, p -value >0.05) while "advanced infection" has a median value of 0.20 (Fig. 4).

3.4.2. Spatial dispersion

The 3 conditions exhibit significant statistical differences between them for t -test value (Kruskal-Wallis test, p -value <0.05) representing whether or not spatial dispersion of IHC stained bacteria follows a specific pattern or is random. "Control" and "early infection" groups do not manifest significant differences between them (Dunn's test, p -value >0.05) while the "advanced infection" group presents a value significantly higher than 0 (Wilcoxon test, p -value <0.05). Values can be found in Table 3 in 7.0 Supplementary Material. A significant positive correlation was found between the proportion of tissue infected by IHC- stained bacteria and t -test values ($\tau = 0.74$, p -value <0.05).

3.4.3. Cluster index

The mean NND ranged from $82.49 \mu\text{m}$ to $8862.10 \mu\text{m}$ with a median value of $243.27 \mu\text{m}$, and from $89.01 \mu\text{m}$ to $8342.25 \mu\text{m}$ with a median value of $849.27 \mu\text{m}$ respectively for the "control" and "early infection" groups. Individuals from the "advanced infection" group had a mean NND ranging from $46.81 \mu\text{m}$ to $64.79 \mu\text{m}$ with a median value of $54.40 \mu\text{m}$ (Fig. 5). Individual values can be found in Table 3 in 7.0 Supplementary Material. A significant difference in mean NND value was observed between individuals from the advanced infection group and the two other groups (Dunn test, p -value <0.05) while the control and early infection group do not present significant differences between them (Dunn test, p -value >0.05). The 3 infection groups exhibited a significant difference in their standard deviation of mean NND (Kruskal- Wallis test, p -value <0.05).

4. Discussion

In this article, a new WSI analysis method to detect, quantify, and characterize IHC-stained *V. aestuarianus* infection in *M. gigas* is presented. The method is based on the detection and analysis of IHC-stained bacteria in each WSI. Different characteristics such as the proportion of tissue area infected, the mean NND, and spatial dispersion of IHC-stained bacteria were analyzed in each image and linked to the level of infection previously measured by qPCR. A significant correlation was found between the quantity of bacteria measured by qPCR and the proportion of tissue infected by IHC-stained bacteria measured by the WSI analysis method.

Levels of bacteria measured by qPCR and exposure duration were weakly correlated. Therefore, grouping the samples according to the level of bacterial infection rather than their exposure duration seems more biologically relevant as *V. aestuarianus* is suspected to have an asynchronous infection behavior, with an initial infection caused by a few bacteria cells present in the hemolymph where the bacteria will multiply until they reach a critical number of pathogenic cells which will then rapidly colonize other tissues (Parizadeh et al., 2018a).

Results obtained by WSI analysis methods generally conformed to the results from the original research by Parizadeh et al. (2018a). Although, the proportion of tissue infected by IHC-stained bacteria was positively related to the mean quantity of bacteria measured by qPCR, the measurements by the two methods were not always aligned. For instance, *V. aestuarianus* was not detected in individuals from the control group by qPCR while small proportions of tissue infected by IHC-stained bacteria were detected in some individuals from the control group with the WSI analysis method. As previously mentioned, these minute signs of IHC-stained bacteria were considered artifacts but

they could have originated from contamination either during experimental infection in the lab, samplings, or tissue labeling. Additional experiments would be required to determine if they were indeed IHC-stained bacteria or not. Similarly, two specimens from the “early infection” group displayed small areas with IHC-stained bacteria, and bacteria-like cells were identified by visual assessment; however, these minute signs of bacterial presence within the tissues were not picked up by qPCR (Table 2). However, this concerns a small proportion of animals, and not more than 0.1 % of their tissues were infected. The opposite was also observed, *V. aestuarianus* was detected by qPCR in some samples but no signs of IHC-stained bacteria were detected in the images (Table 1).

These small discrepancies observed between qPCR results and the results obtained by WSI analysis could arise from multiple factors. Bacteria level measured by qPCR was obtained by determining the mean value of results from different tissue DNAs (gills, digestive gland, mantle, muscle, labial palp). But as previously mentioned, *V. aestuarianus* is suspected to have an asynchronous infection pattern and therefore, its spread might not be homogenous through the different tissues. In addition, for the WSI analysis, an animal cross-section does not always contain the same proportion of the different tissues, some organs might be under or over-represented in some images (Zarella et al., 2019). Therefore the quantity of bacteria assessed by WSI analysis might be biased by the nature and the proportion of the tissues represented in the WSI. Another factor to consider is that some bacteria might be washed away during histological preparation, particularly because of the poor conservation of circulatory fluids – haemolymph –, therefore bacterial infection assessment made by WSI analysis might be underestimated. Finally, the qPCR method can detect as few as 10^3 bacteria from small pieces of tissues (mg) but this analytical threshold can limit bacterial detection in early infection phases (Saulnier et al., 2009). Although methods based on DNA detection are more sensitive than IHC-based methods, IHC plays a crucial role in the diagnosis of certain pathologies (Burge et al., 2016). While the choice between qPCR and IHC depends on the specific marker being assessed and the experimental context, combining these advanced molecular and cellular techniques, allows for the confirmation of both the identity and quantity of pathogens (Arevalo et al., 2024; Oumarou Hama et al., 2022; Burge et al., 2016).

Despite these potential limitations, this finding supports the claim that this new method based on WSI analysis might be complementary to the qPCR method to assess bacterial infection levels by *V. aestuarianus* in *M. gigas*.

Mean NND and dispersion index were used to characterize bacterial localization during infection progression in the tissues. These two indicators were positively correlated to the proportion of tissue infected by IHC-stained bacteria as well as the quantity of bacteria measured by qPCR. The difference in mean NND indicates that in the advanced infection stage bacteria tended to be more clustered than in the early infection stage (Fig. 5). It supports the actual pathogenesis model for *V. aestuarianus* associated disease. That is that *V. aestuarianus* tends to develop in clusters with increased bacterial infection (Parizadeh et al., 2018a). With this quantitative imaging approach, we are now able to propose a spatial representation of disease progression characterizing the spatial dynamics of infection of *M. gigas* by *V. aestuarianus* on a fine scale. Pathogenesis induced by *V. aestuarianus* in *M. gigas* can be described in several successive stages: (1) initial penetration and colonization (2) bacterial multiplication at entry sites (3) dispersion and invasion of connective tissues. Finally, the progression of the disease is associated with an increase in bacterial clusters in all the animal tissues, confirming the septicemic characteristics of *V. aestuarianus* infection (Fig. 6).

4.1. Limitations and potential ways for improvement

Digital pathology offers several potential benefits over traditional histopathological methods and provides solutions to some of the key issues associated with the manual assessment of tissue samples (Madabhushi and Lee, 2016).

A potential way to improve the method would be to analyze the different tissues separately using a tissue detection method before performing the analysis (Bandi et al., 2017). It could potentially help refine bacterial infection patterns at the tissue level instead of cross-section as it is now, and it could bring more insight into pathogenesis and intra/ inter-organ infection patterns.

However, limitations inherent to digital slide image analysis need to be addressed before further development of the method and its adoption into routine procedures. Pre-analytical steps are prone to artifact generation including poor microtomy (thickness variances, knife chatter), improper tissue placement (folding, tearing, air bubbles), or improper staining procedure (over or under-staining, stain batch variation) (Aeffner et al., 2017). Histological slide digitization also represents another potential source of artifact generation, such as blurriness, lighting, and contrast issues (Mulrane et al., 2008). Most of these pre-analytical steps can be automated and standardized to decrease the degree of variability and the odds of artifact generation (Webster and Dunstan, 2014). Therefore, process automation and standardization should be encouraged in routine analysis, along with appropriate quality control procedures to assess potential bias throughout the workflow (Aeffner et al., 2019). Ideally, an experienced pathologist should stay involved in the whole analysis and perform different quality control procedures along the workflow to assess the influence of the different factors potentially interfering with the analysis (Carnegie et al., 2016). Another limitation comes from the problem of estimating the abundance of IHC stains in histological tissue. As previously mentioned, the color range defined by upper and lower HSV values to detect IHC-stained bacteria is arbitrary and relies only on expert assessment. Extending or on the contrary reducing the color range threshold will affect the number of pixels detected and ultimately the estimation of the area covered by IHC-stained bacteria in the images. Threshold values used for tissue detection and IHC detection are subjective. The chosen parameters were the ones giving the most satisfactory results in terms of tissue detection, artifact removal, and IHC detection according to the operator. As it has been extensively documented, visual assessment by pathologists can be influenced by inherent cognitive and visual biases (Wolf et al., 2015). Therefore, running a sensitivity test on each of these parameters could help to build more objective tools to set these parameters. Further research should be carried out to validate the assumption that IHC-stained bacteria detected on the slide are representative and, in some way, quantitatively related to the abundance of the antigen present in the tissue section, which in turn is related to the absolute number of bacteria in the original tissue (Taylor and Levenson, 2006). Moreover, this method quantifies bacterial localization during disease progression only on a small portion of the organ as a 2D slide is not representative of the complexity of an entire organ. Bacterial infection dynamics in an organ and a whole organism might be more complex than what the method can reveal from a single cross-section.

Although there are inherent biases in this method, if acknowledged and taken into consideration, these might not limit its use as the results could be considered relative and not absolute. Another important aspect of the methodology presented here is that it relies solely on open-source software, and the code was made publicly available through an online repository (<https://github.com/Valentin-Geslin/oyster>). The use of open-source and open-access material was done to promote the development and use of such WSI analysis methods.

With respect to the results presented here, this new method complements the traditionally used qPCR method to detect and quantify bacterial infection by *V. aestuarianus* in *M. gigas* because it allows a better understanding of the extent of bacterial spread through the tissues. Its usage could potentially be adopted in routine tests to improve detection and extent of *V. aestuarianus* outbreaks in aquaculture facilities. However, pre-analytical steps in WSI preparation need to be standardized as these steps are prone to artifact generation and may result in variability in the outcome. Further research should also be carried out on the early infection phase to elucidate the dissimilarity between bacterial quantity measured by qPCR and of tissue infected as determined by IHC staining analysis.

Implementation of the WSI analysis-based method is a multifaceted and inherently multidisciplinary endeavor requiring contributions from different fields. Improved understanding of current challenges to implementation, as well as the benefits of this kind of method, can help prospective users identify the best means to achieve their goals.

CRedit authorship contribution statement

Valentin Geslin: Writing – review & editing, Writing – original draft, Visualization, Validation, Methodology, Investigation, Formal analysis, Conceptualization. **Leila Parizadeh:** Writing – review & editing, Writing – original draft, Visualization, Formal analysis, Conceptualization. **Marie-Agnes Travers:** Writing – review & editing, Supervision,

Formal analysis, Conceptualization. **Luca Tomasetti**: Writing – review & editing, Validation. **Thor Ole Gulsrud**: Writing – review & editing, Supervision. **Declaration of competing interest**

The authors declare that they have no known competing financial interests or personal relationships that could have appeared to influence the work reported in this paper.

Acknowledgment

Thanks to Celine Garcia and Bruno Chollet from Ifremer station “La Tremblade” for their help and feedback. This study is set within the framework of the « Laboratoire d’Excellence (LabEx) » TULIP (ANR-10- LABX-41).

Appendix A. Supplementary data

Supplementary data to this article can be found online at <https://doi.org/10.1016/j.aquaculture.2024.741983>

Data availability

Data will be made available on request.

TABLE 1

Some tiles from different tissues sorted by condition. On original tiles, different tissues (gills, digestive gland, mantle, abductor muscle, labial palp) are visible with IHC-stained bacteria (pink color) when infected. Masked tiles display only IHC-stained bacteria if present in the original tile.

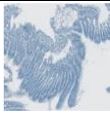
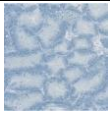

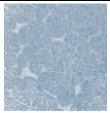
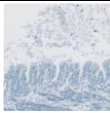


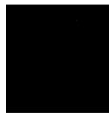


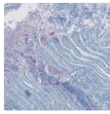

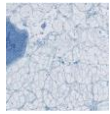
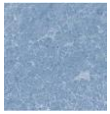
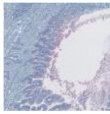


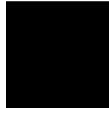


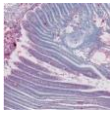

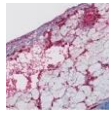
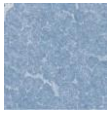
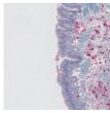
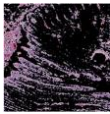

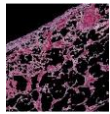

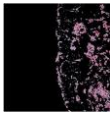
Infection status	Tile	Gills	Digestive gland	Mantle	Abductor's muscle	Labial palp
Control	Original tile					
	Masked tile					
Early infection	Original tile					
	Masked tile					
Advanced infection	Original tile					
	Masked tile					

TABLE 2

Examples of tiles from the control group showing evidence of bacterial infection and their respective mask.

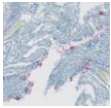

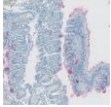



Image	Infection status	Original tile	Masked tile
16,049-8-3,401,002	Control		
16,049-8-3,401,002	Control		
16,049-6-3,301,002	Control		

FIGURE 1

General workflow of the WSI analysis method. WSIs were fragmented into tiles for IHC detection analysis. In parallel, tissue detection is performed to get the overall tissue area per image to compute the proportion of tissue area infected by IHC-stained bacteria. IHC-stained bacteria particles were extracted from the WSI and used to perform colocalization and spatial distribution analysis.

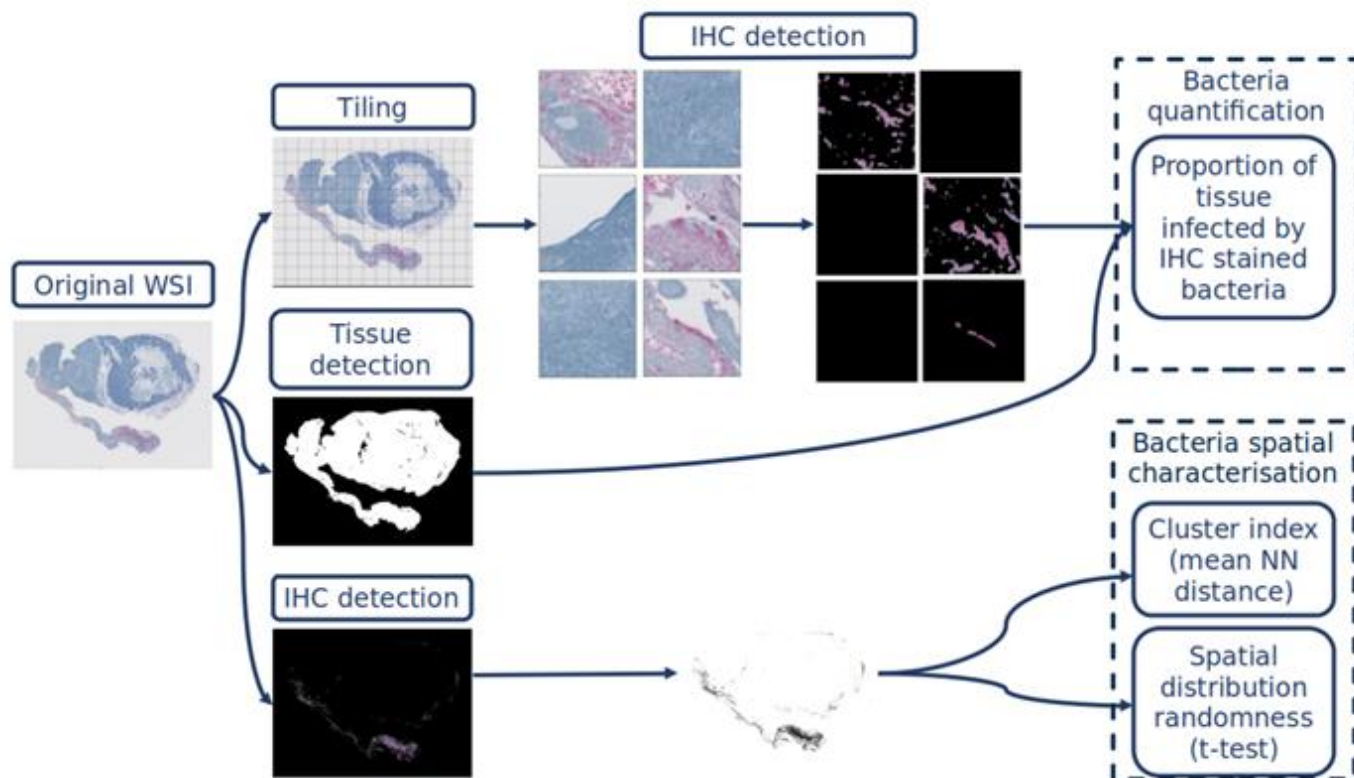


FIGURE 2

Quantity of bacteria cells (log10) per 25 ng of total DNA (left) and proportion of tissue area (%) infected by IHC stained bacteria per images and for the different groups (right). The mean values of the quantity of bacteria cells for the control, early infection, and advanced infection groups were respectively 0, 0.46, and 6.82. The mean quantity of bacteria cells from the control and early infection group was not significantly different from 0 (Wilcoxon test, p -value <0.05), and the advanced infection group was significantly higher than the 2 other groups (Dunn's test, p -value >0.05). The mean values of the proportion of tissue infected by IHC- stained bacteria for control, early infection, and advanced infection group are respectively 0 %, 0.005 %, and 13.20 %. The proportion of tissue area infected by IHC- stained bacteria for the advanced infection group was significantly higher than the 2 other groups (Dunn's test, p -value >0.05). The advanced infection group significantly stands out from the 2 other groups for the quantity of bacteria cells (log10) per sample and the proportion of tissue area (%) infected by IHC-stained bacteria per image.

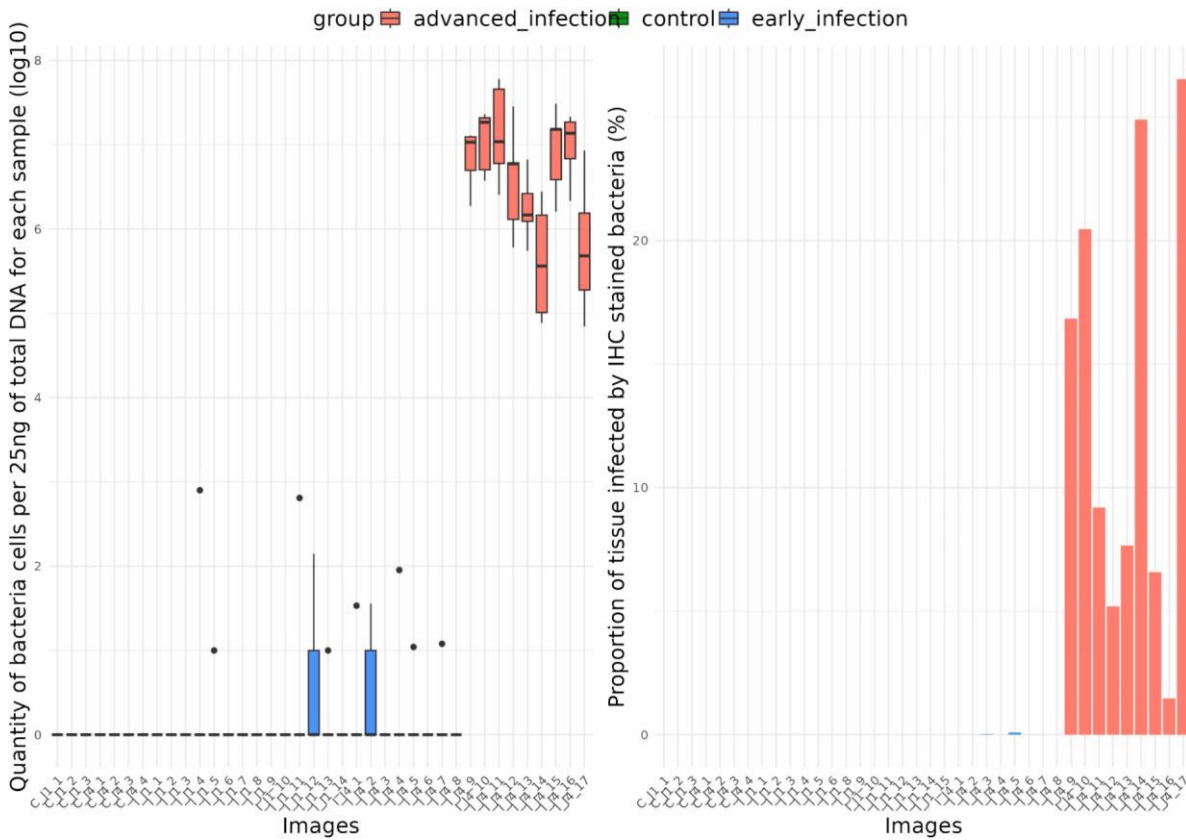


FIGURE 3

Relationship between proportion of tissue infected by IHC stained bacteria and mean quantity of bacteria (log10) per image and category. Control and early infection samples display a relatively low proportion of tissue infected by IHC-stained bacteria (min = 0 %, max = 0.09 %) and mean quantity of bacteria cells (min =0, max = 2.20) compared to the advanced infection group where values from the proportion of tissue infected by IHC stained bacteria range from 1.47 % to 26.53 % and values from mean quantity of bacteria (log10) range from 6.01 to 7.39. The overall F-value of the logarithmic regression model is 43.91 with a corresponding p-value lower than 0.05, which indicates that the model fits the data.

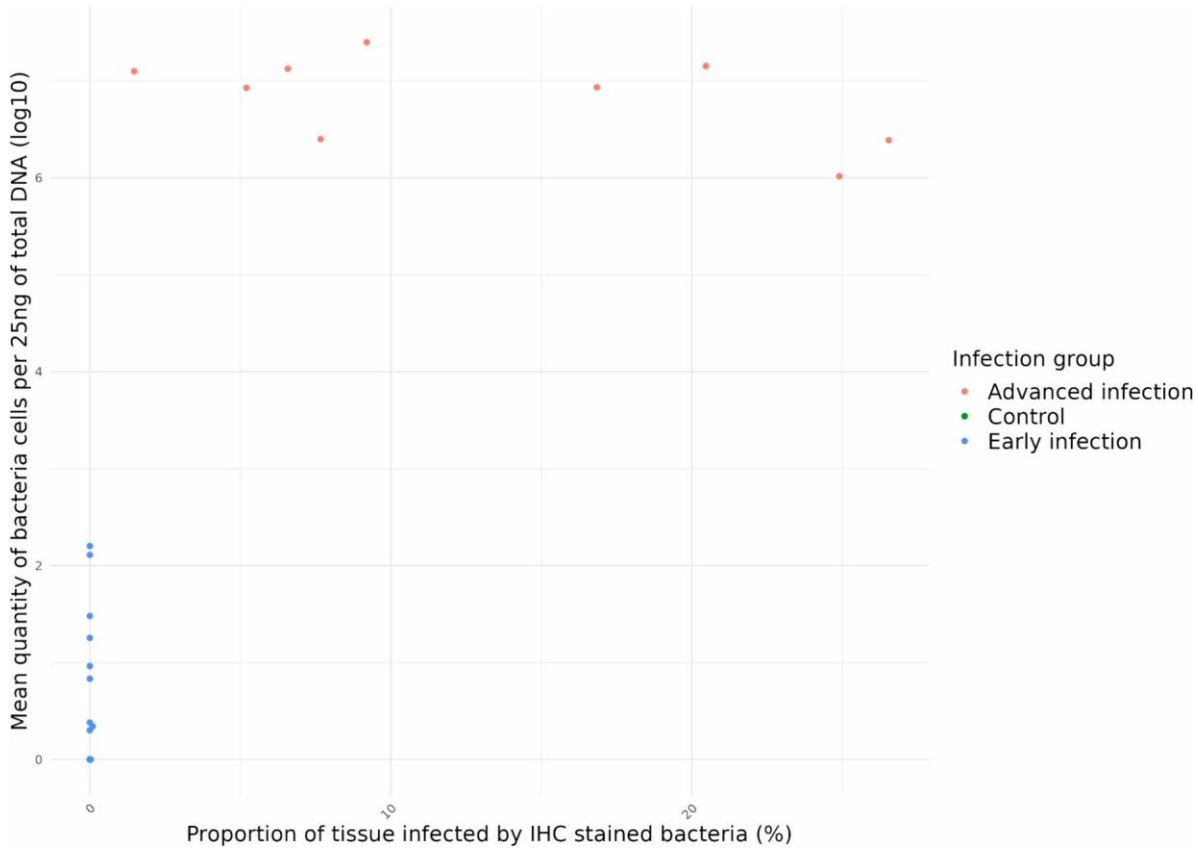


FIGURE 4

Pearson's coefficient value per image and category. Pearson's coefficient value for the control and early infection cohort ranged from 0.006 to 0.02, while for the advanced infection group, Pearson's coefficient value ranged from 0.07 to 0.35 with a median value of 0.20.

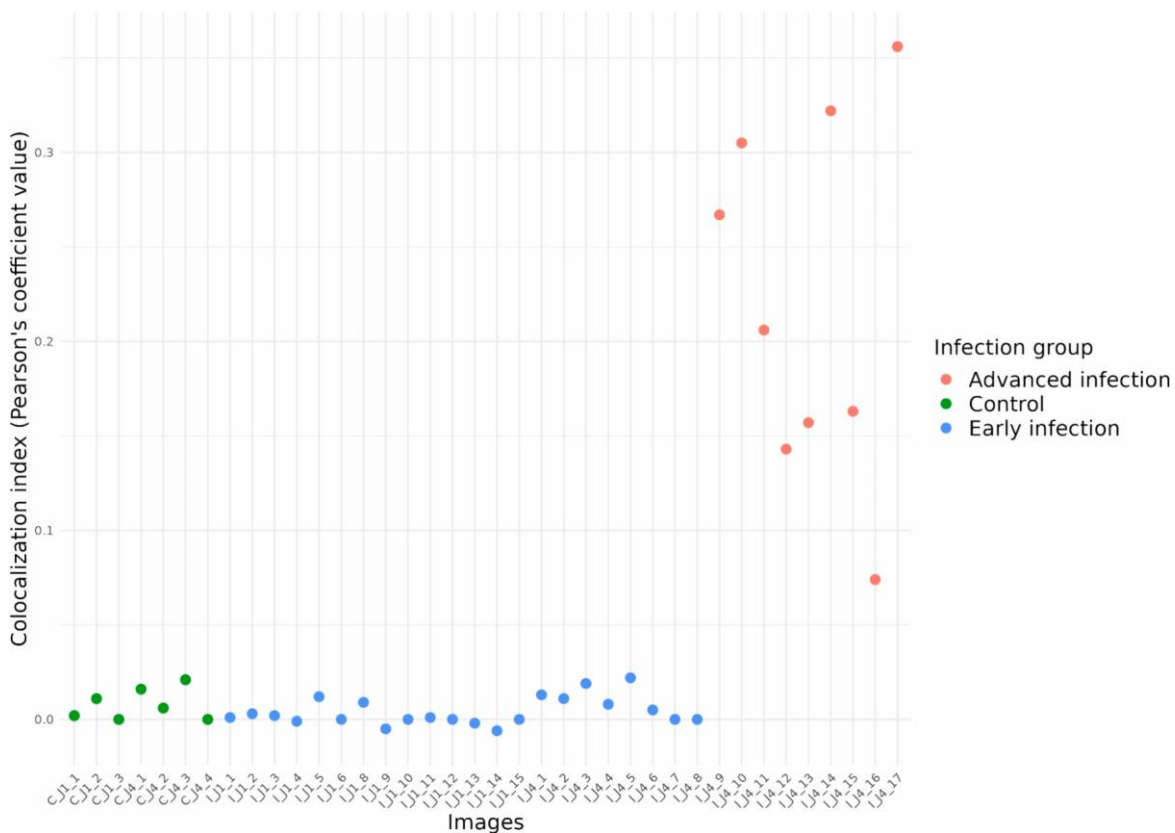


FIGURE 5

Distribution of mean nearest neighbor distance (NND) between particles per sample infection status (left) and mean NND (with standard deviation) between particles per image and category (right). The mean NND between particles for the control and early infection cohort ranged from 82.49 μm to 8862.10 μm , while for the advanced infection group values ranged from 46.81 μm to 64.79 μm with a median value of 54.40 μm .

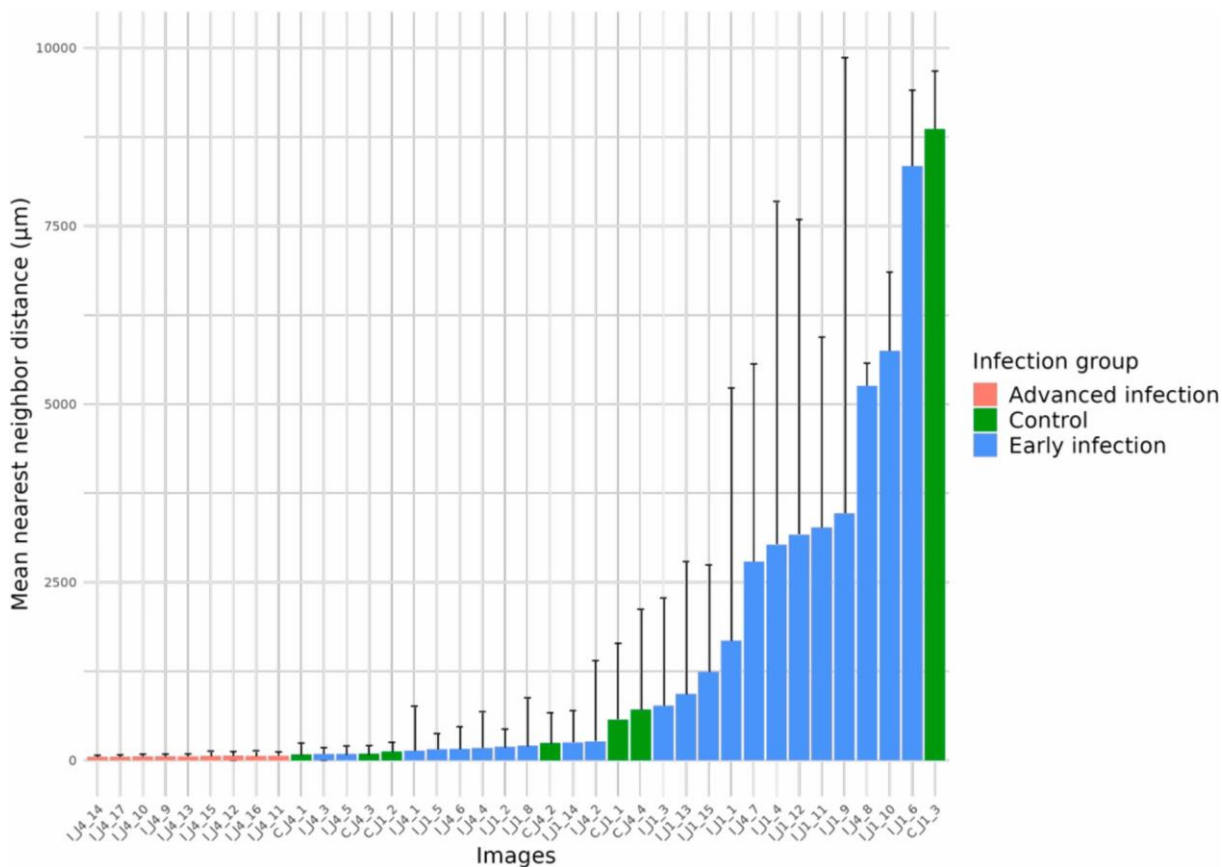
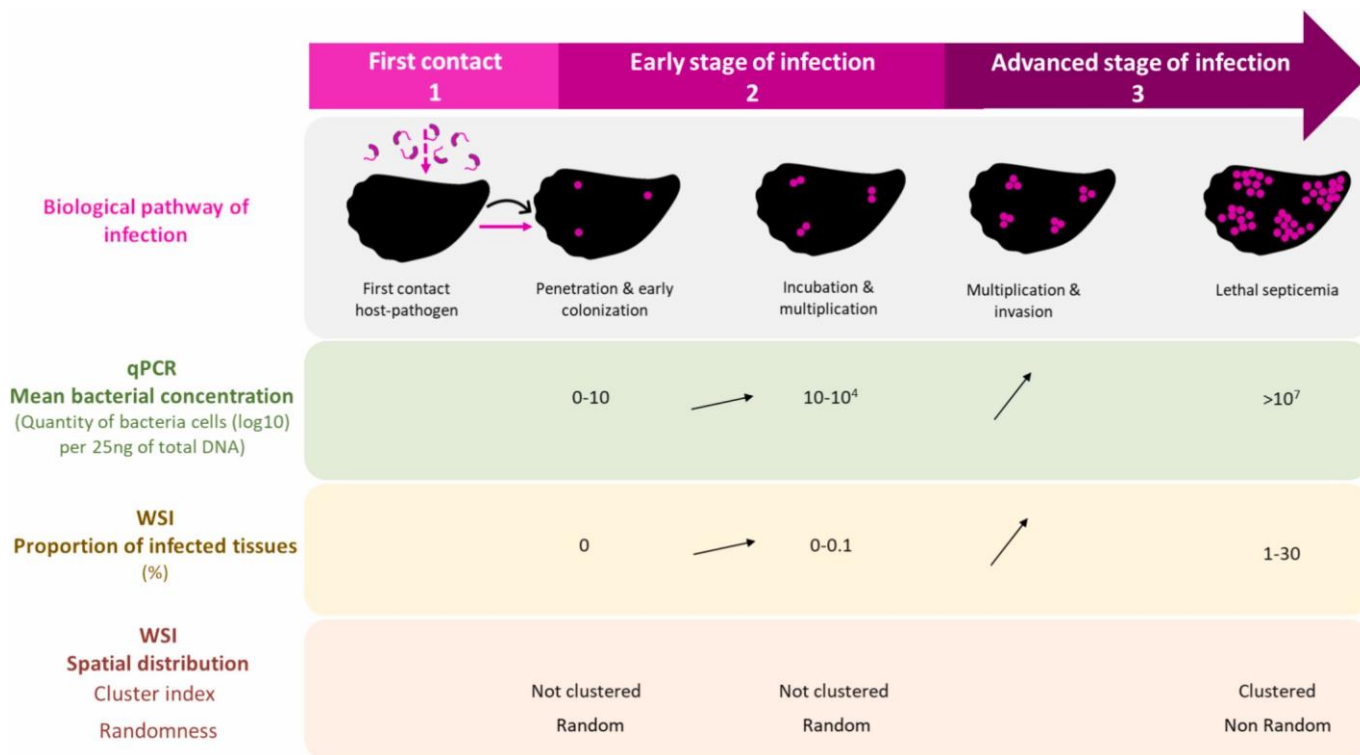


FIGURE 6

Schematic representation of the different stages of pathogenesis and biological pathway of infection induced by *V. aestuarianus* in *M. gigas* based on the WSI method combined with Qpcr.



References

- Aeffner, F., Wilson, K., Martin, N.T., Black, J.C., Hendriks, C.L.L., Bolon, B., Rudmann, D. G., Gianani, R., Koegler, S.R., Krueger, J., Young, G.D., 2017. The gold standard paradox in digital image analysis: manual versus automated scoring as ground truth. *Arch. Pathol. Lab Med.* 141 (9), 1267–1275.
- Aeffner, F., Zarella, M.D., Buchbinder, N., Bui, M.M., Goodman, M.R., Hartman, D.J., Lujan, G.M., Molani, M.A., Parwani, A.V., Lillard, K., Turner, O.C., 2019. Introduction to digital image analysis in whole-slide imaging: a white paper from the digital pathology association. *J Pathol Informatics* 10 (1), 9.
- Arevalo, F., Rayme, S., Ramírez, R., Rolando, R., Fustamante, J., Monteghirfo, M., Chavez, R., Monge, E., 2024. Immunohistochemistry and real-time polymerase chain reaction: importance in the diagnosis of intestinal tuberculosis in a Peruvian population. *BMC Gastroenterol.* 24 (1), 166.
- Arzul, I., Corbeil, S., Morga, B., Renault, T., 2017. Viruses infecting marine molluscs. *J. Invertebr. Pathol.* 147, 118–135.
- Arzul, I., Garcia, C., Chollet, B., Serpin, D., Lupo, C., Noyer, M., Tourbiez, D., Berland, C., Degremont, L., Travers, M.A., 2022. First characterization of the parasite *Haplosporidium costale* in France and development of a real-time PCR assay for its rapid detection in the Pacific oyster, *Crassostrea gigas*. *Transbound. Emerg. Dis.* 69 (5), e2041–e2058.
- Axen, C., Carnegie, R., Cheslett, D., Jones, S., Kristmundsson, A., Kvamme, B., Lillehaug, A., Madsen, L., Munro, E., Paley, R., Powell, M., 2019. Working Group on Pathology and Diseases of Marine Organisms (WGPDMO).
- Bandi, P., Van De Loo, R., Intezar, M., Geijs, D., Ciompi, F., Van Ginneken, B., Van Der Laak, J., Litjens, G., 2017. Comparison of different methods for tissue segmentation in histopathological whole-slide images. In: In 2017 IEEE 14th International Symposium on Biomedical Imaging (ISBI 2017). IEEE, pp. 591–595.
- Barange, M., Bahri, T., Beveridge, M.C., Cochrane, K.L., Funge-Smith, S., Poulain, F., 2018. Impacts of climate change on fisheries and aquaculture. *United Nations' Food and Agriculture Organization* 12 (4), 628–635.
- Ben-Horin, T., Burge, C.A., Bushek, D., Groner, M.L., Proestou, D.A., Huey, L.I., Bidegain, G., Carnegie, R.B., 2018. Intensive oyster aquaculture can reduce disease impacts on sympatric wild oysters. *Aquac. Environ. Interact.* 10, 557–567.
- Berg, C., Vågsholm, I., Willeberg, P., 2015. Oyster mortality. *EFSA J.* 13 (6).
- Bolte, S., Cordelieres, F.P., 2006. A guided tour into subcellular colocalization analysis in light microscopy. *J. Microsc.* 224 (3), 213–232.
- Boyd, C.E., Clay, J.W., 1998. Shrimp aquaculture and the environment. *Sci. Am.* 278 (6), 58–65.
- Brocher, J., 2022. Biovoxxel/BioVoxel-toolbox: BioVoxel toolbox. *Zenodo* 6, 10–5281.
- Burge, C.A., Friedman, C.S., Getchell, R., House, M., Lafferty, K.D., Mydlarz, L.D., Prager, K.C., Sutherland, K.P., Renault, T., Kiryu, I., Vega-Thurber, R., 2016. Complementary approaches to diagnosing marine diseases: a union of the modern and the classic. *Philos. Trans. R. Soc. B* 371 (1689), 20150207.
- Burge, C.A., Shore-Maggio, A., Rivlin, N.D., 2017. Ecology of emerging infectious diseases of invertebrates. *Ecol. of Invertebrate Diseases* 587–625.
- Carnegie, R.B., Arzul, I., Bushek, D., 2016. Managing marine mollusc diseases in the context of regional and international commerce: policy issues and emerging concerns. *Philosophical Transactions of the Royal Society B: Biological Sciences* 371 (1689), 20150215.
- Castinel, A., Fletcher, L., Dhand, N., Rubio, A., Whittington, R., Taylor, M., 2015. OsHV-1 Mortalities in Pacific Oysters in Australia and New Zealand: The farmer's Story. Report Prepared for the Ministry of Business, Innovation and Employment (MBIE). Cawthron Report, p. 2567.
- Chaney, M.L., Gracey, A.Y., 2011. Mass mortality in Pacific oysters is associated with a specific gene expression signature. *Mol. Ecol.* 20 (14), 2942–2954.
- Elston, R.A., 1993. Infectious diseases of the Pacific oyster, *Crassostrea gigas*. *Annu. Rev. Fish Dis.* 3, 259–276.
- F.A.O., Fisheries, 2022. The state of world fisheries and aquaculture: towards blue transformation.

- Fuhrmann, M., Castinel, A., Cheslett, D., Whittington, R.J., 2019. L'impact des microvariants du virus herpétique *Ostreid herpesvirus 1* sur la culture d'huîtres creuses dans les hémisphères Nord et Sud depuis 2008. *Revue Scientifique et Technique (International Office of Epizootics)* 38 (2), 491–509.
- Garnier, M., Labreuche, Y., Garcia, C., Robert, M., Nicolas, J.L., 2007. Evidence for the involvement of pathogenic bacteria in summer mortalities of the Pacific oyster *Crassostrea gigas*. *Microb. Ecol.* 53, 187–196.
- Garrabou, J., Gomez-Gras, D., Medrano, A., Cerrano, C., Ponti, M., Schlegel, R., Bensoussan, N., Turicchia, E., Sini, M., Gerovasileiou, V., Teixido, N., 2022. Marine heatwaves drive recurrent mass mortalities in the Mediterranean Sea. *Glob. Chang. Biol.* 28 (19), 5708–5725.
- Green, T.J., Vergnes, A., Montagnani, C., De Lorigeril, J., 2016. Distinct immune responses of juvenile and adult oysters (*Crassostrea gigas*) to viral and bacterial infections. *Vet. Res.* 47, 1–11.
- Griffiths, D., Pratoomyot, J., Vu, N.T., Jiravanichpaisal, P., Shinn, A.P., Briggs, M., Trong, T.Q., 2018. Asian shrimp production and the economic costs of disease. *Asian Fisheries Sci. J.* 31.
- Janowczyk, Andrew, Ren Zuo, Hannah Gilmore, Feldman, Michael, 2019. and Anant Madabhushi. "HistoQC: an open-source quality control tool for digital pathology slides." *JCO clinical cancer informatics* 3, 1–7.
- Kalkan, S., Altug, G., 2020. The composition of cultivable bacteria, bacterial pollution, and environmental variables of the coastal areas: an example from the southeastern Black Sea, Turkey. *Environ. Monit. Assess.* 192 (6), 356.
- Kathijotes, N., Alam, L., Kontou, A., 2015. Aquaculture, Coastal Pollution and the Environment. *Aquaculture Ecosystems. Adaptability and Sustainability*, pp. 139–163.
- Lagache, T., Sauvonnet, N., Danglot, L., Olivo-Marin, J.C., 2015. Statistical analysis of molecule colocalization in bioimaging. *Cytometry A* 87 (6), 568–579.
- Landos, M., Smith, M.L., Immig, J., 2021. Aquatic Pollutants in Oceans and Fisheries. IPEN.
- Li, X., Shi, C., Yang, B., Li, Q., Liu, S., 2023. High temperature aggravates mortalities of the Pacific oyster (*Crassostrea gigas*) infected with *Vibrio*: a perspective from homeostasis of digestive microbiota and immune response. *Aquaculture* 568, 739309.
- Lupo, C., Osta Amigo, A., Fleury, E., Robert, S., Garcia, C., Arzul, I., Baillon, L., Bechemin, C., Canier, L., Chollet, B., Dechamps, L., 2016. Bilan 2015 du dispositif national de surveillance de la santé des mollusques marins.
- Madabhushi, A., Lee, G., 2016. Image analysis and machine learning in digital pathology: challenges and opportunities. *Med. Image Anal.* 33, 170–175.
- McCombie, H., Samain, J.F., 2007. Summer Mortality of Pacific Oyster *Crassostrea gigas*: The Morest Project.
- Mulrane, L., Rexhepaj, E., Penney, S., Callanan, J.J., Gallagher, W.M., 2008. Automated image analysis in histopathology: a valuable tool in medical diagnostics. *Expert. Rev. Mol. Diagn.* 8 (6), 707–725.
- Noger-Huet, E., Vagner, M., Le Grand, F., Graziano, N., Bideau, A., Brault-Favrou, M., Churlaud, C., Bustamante, P., Lacoue-Labarthe, T., 2022. Risk and benefit assessment of seafood consumption harvested from the Pertuis Charentais region of France. *Environ. Pollut.* 292, 118388.
- Oumarou Hama, H., Aboudharam, G., Barbieri, R., Lepidi, H., Drancourt, M., 2022. Immunohistochemical diagnosis of human infectious diseases: a review. *Diagn. Pathol.* 17 (1), 17.
- Palacios, G., Lovoll, M., Tengs, T., Hornig, M., Hutchison, S., Hui, J., Kongtorp, R.T., Savji, N., Bussetti, A.V., Solovyov, A., Kristoffersen, A.B., 2010. Heart and skeletal muscle inflammation of farmed salmon is associated with infection with a novel reovirus. *PLoS One* 5 (7), e11487.
- Pantanowitz, L., Valenstein, P.N., Evans, A.J., Kaplan, K.J., Pfeifer, J.D., Wilbur, D.C., Collins, L.C., Colgan, T.J., 2011. Review of the current state of whole slide imaging in pathology. *J Pathol Informatics* 2 (1), 36.
- Parizadeh, L., Tourbiez, D., Garcia, C., Haffner, P., Degremont, L., Le Roux, F., Travers, M.A., 2018a. Ecologically realistic model of infection for exploring the host damage caused by *Vibrio aestuarianus*. *Environ. Microbiol.* 20 (12), 4343–4355.
- Parizadeh, L., Travers, M.A., Garcia, C., Chollet, B., 2018b. Tissue Damage and Tissue Localisation of the bacteria *Vibrio aestuarianus* during an Experimental Infection (*Crassostrea gigas*).
- Paul-Pont, I., Dhand, N.K., Whittington, R.J., 2013. Spatial distribution of mortality in Pacific oysters *Crassostrea gigas*: reflection on mechanisms of OsHV-1 transmission. *Dis. Aquat. Org.* 105 (2), 127–138.

- Petrosillo, I., Scardia, A.M.S., Ungaro, N., Specchiulli, A., Fanelli, G., Centoducati, G., De Serio, F., Carlucci, R., Valente, D., Barbone, E., Pini, A., 2023. Towards sustainable marine spatial planning of aquaculture. *Ecol. Indic.* 154, 110542.
- Saulnier, D., De Decker, S., Haffner, P., 2009. Real-time PCR assay for rapid detection and quantification of *Vibrio aestuarianus* in oyster and seawater: a useful tool for epidemiologic studies. *J. Microbiol. Methods* 77 (2), 191–197.
- Taylor, C.R., Levenson, R.M., 2006. Quantification of immunohistochemistry: issues concerning methods, utility and semiquantitative assessment II. *Histopathology* 49 (4), 411–424.
- Webster, J.D., Dunstan, R.W., 2014. Whole-slide imaging and automated image analysis: considerations and opportunities in the practice of pathology. *Vet. Pathol.* 51 (1), 211–223.
- Whittington, R.J., Liu, O., Hick, P.M., Dhand, N., Rubio, A., 2019. Long-term temporal and spatial patterns of *Ostreid herpesvirus 1* (OsHV-1) infection and mortality in sentinel Pacific oyster spat (*Crassostrea gigas*) inform farm management. *Aquaculture* 513, 734395.
- Wolf, J.C., Baumgartner, W.A., Blazer, V.S., Camus, A.C., Engelhardt, J.A., Fournie, J.W., Frasca Jr., S., Groman, D.B., Kent, M.L., Khoo, L.H., Law, J.M., 2015. Nonlesions, misdiagnoses, missed diagnoses, and other interpretive challenges in fish histopathology studies: a guide for investigators, authors, reviewers, and readers. *Toxicol. Pathol.* 43 (3), 297–325.
- Wright, A., Li, X., Yang, X., Soto, E., Gross, J., 2023. Disease prevention and mitigation in US finfish aquaculture: a review of current approaches and new strategies. *Rev. Aquac.* 15 (4), 1638–1653.
- Yang, B., Zhai, S., Li, X., Tian, J., Li, Q., Shan, H., Liu, S., 2021. Identification of *Vibrio alginolyticus* as a causative pathogen associated with mass summer mortality of the Pacific oyster (*Crassostrea gigas*) in China. *Aquaculture* 535, 736363.
- Zarella, M.D., Bowman, D., Aeffner, F., Farahani, N., Xthona, A., Absar, S.F., Parwani, A., Bui, M., Hartman, D.J., 2019. A practical guide to whole slide imaging: a white paper from the digital pathology association. *Arch. Pathol. Lab Med.* 143 (2), 222–234.